Journal of Alloys and Compounds 520 (2012) 266–271

Contents lists available at SciVerse ScienceDirect

Journal of Alloys and Compounds

journal homepage: www.elsevier.com/locate/jallcom

Preparation and magnetic properties of Fe_3O_4 microparticles with adjustable size and morphology

Rufen Chen*, Jianhui Cheng, Yu Wei*

College of Chemistry and Material Science, Hebei Normal University, Shijiazhuang, Hebei 050016, China

ARTICLE INFO

Article history:
Received 20 September 2011
Received in revised form 4 January 2012
Accepted 5 January 2012
Available online 14 January 2012

Keywords:
Fe_3O_4 microparticles
Adjustable size
Crystal morphology
Hydrothermal method
Magnetic properties

ABSTRACT

Homogeneous magnetite (Fe_3O_4) microparticles with adjustable morphologies and sizes were successfully prepared using a simple hydrothermal method. The resulting products were pure Fe_3O_4 with face-centered cubic structures. The morphology and size of Fe_3O_4 depended on the concentration of sodium hydroxide (NaOH) and ethanediol ($C_2H_6O_2$). Fe_3O_4 microoctahedrons were formed when the concentration of NaOH ranged from 0.30 to 0.75 M. The size of the octahedral Fe_3O_4 particles decreased and the morphology changed from octahedral to cubic when the amount of $C_2H_6O_2$ was increased. The octahedral and cubic Fe_3O_4 exhibited single-crystal features. The as-prepared Fe_3O_4 microparticles with various morphologies and sizes displayed ferromagnetic behaviors.

1. Introduction

Magnetite (Fe_3O_4) has been widely studied because of its fascinating properties and wide range of potential applications in magnetic recording media, ferrofluids, and as a catalyst [1–4]. The shape and size of Fe_3O_4 crystals determine their chemical and physical properties, which may serve as a foundation for the development of new fields [5,6]. The exploration of the methods for synthesizing magnetic microcrystals with desired morphology and size has been of scientific and technological interest [7]. Employing various methods, the Fe_3O_4 with different morphologies have been successfully synthesized, such as spheres [8–11], octahedrons [12–17], cubes [18,7], tetrakaidecahedrons [19], wires [20,21], fractals [22], dendrites [23], hollow structures [24], urchin-like structures [5], nanosheets [1,25], and nanoprisms [26]. However, fine shape control of Fe_3O_4 microparticles through a simple synthesis process with good size and shape-dependent properties remains a difficult task [27]. Recently, Zhao and co-workers [28] synthesized different morphological single-crystal Fe_3O_4 by a polyol method in ethylene glycol at 200 °C. Zhang et al. [15] prepared different morphological Fe_3O_4 by a thermal decomposition method using $Fe(acac)_3$ precursor. Although well-defined Fe_3O_4 crystals with different morphologies have been synthesized by relative simple methods [15,27–29], it is still a great challenge to further develop simple and low-cost approaches for the synthesis of homogeneous Fe_3O_4 microparticles with variable shapes and sizes. To the best of our knowledge, the controlled preparation of Fe_3O_4 microparticles with adjustable morphologies and sizes by changing the ratio between NaOH and $C_2H_6O_2$ in aqueous solution has not hitherto been reported.

In the current study, homogeneous Fe_3O_4 microparticles with adjustable sizes and morphologies were prepared by a simple, cheap and harmless ethanediol ($C_2H_6O_2$)-assisted hydrothermal process using potassium ferricyanide ($K_3Fe(CN)_6$), hydrazine hydrate ($N_2H_4{\cdot}H_2O$), and sodium hydroxide (NaOH). Well-defined Fe_3O_4 microcrystals with different sizes and morphologies (octahedral and cubic) have been successfully synthesized by adjusting the concentration of NaOH and $C_2H_6O_2$.

2. Experimental

2.1. Materials

Potassium ferricyanide ($K_3Fe(CN)_6$), sodium hydroxide (NaOH), ethanediol ($C_2H_6O_2$) and hydrazine hydrate ($N_2H_4{\cdot}H_2O$) were purchased from Tianjin Chemical Reagents Company (the purities are 99%), and were used as received without further purification. Distilled water was used as solvent for the reactions.

2.2. Synthesis of Fe_3O_4 microparticles

$K_3Fe(CN)_6$ (1.6463 g) was dissolved in 50 mL distilled water under stirring. The resulting solution was mixed with 0–10 mL NaOH solution (6 M), 5 mL $N_2H_4{\cdot}H_2O$, and an appropriate amount of $C_2H_6O_2$ solution (0–20 mL). The concentration range of NaOH in the mixtures was 0–1.00 M. The mixtures were stirred for 10 min, and then transferred into a 100 mL Teflon-lined stainless steel autoclave, which was

* Corresponding authors. Tel.: +86 031186268342; fax: +86 031186268342.
E-mail addresses: rufenchen7@gmail.com (R. Chen), weiyu@mail.hebtu.edu.cn (Y. Wei).

0925-8388/$ – see front matter © 2012 Elsevier B.V. All rights reserved.
doi:10.1016/j.jallcom.2012.01.039

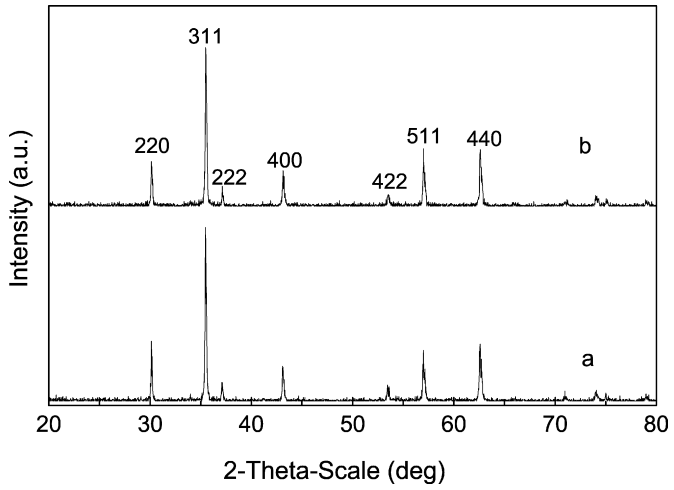

Fig. 1. XRD patterns of octahedral and cubic Fe_3O_4 microcrystals obtained in the presence of 0.50 M NaOH and different volumes of $C_2H_6O_2$ (5 mL and 20 mL) (a: octahedral; b: cubic).

sealed and maintained at 180 °C for 4–16 h. The black-colored solid product was collected via magnetic filtration and washed several times with distilled water and ethanol. The final product was dried in a vacuum oven at 50 °C for 12 h.

2.3. Characterization

X-ray diffraction (XRD) patterns were obtained on a Bruker diffractometer D8 ADVANCE using a Cu Kα radiation. The field emission scanning electron microscopy (FESEM) were conducted on a Philips XL-30 field-emission scanning electron microscope operated at 20 kV, while the transmission electron microscopy (TEM) and the selected area electron diffraction (SAED) were carried out on a JEOL-JEM-2010 at 200 kV. The magnetic measurement of the products was carried out in a vibrating sample magnetometer (VSM-7310, Lakeshore, USA). Magnetic hysteresis loops were recorded at room temperature by first saturating the sample in a field of 10,000.0 Oe, and then the saturation magnetization (M_s), the remanent magnetization (M_r), and the coercivity (H_c) were determined for the sample.

3. Results and discussion

3.1. Structural features

X-ray diffraction (XRD) was performed to investigate the crystalline structure of the octahedral and cubic Fe_3O_4 microcrystals. The octahedral and cubic Fe_3O_4 microcrystals were obtained at 180 °C for 16 h in the presence of 0.50 M NaOH and different volumes of $C_2H_6O_2$ solution (5 mL and 20 mL). Fig. 1 shows the XRD patterns of the octahedral and cubic Fe_3O_4 microcrystals. The reflection peaks match the reported peaks of pure Fe_3O_4 (JCPDS No. 82-1533) and can be ascribed to its face-centered cubic (fcc) structure. The corresponding values of the refined unit cell parameter, 8.394 and 8.397 Å, are in good agreement with the reported data for Fe_3O_4 (8.396 Å) [30–32].

3.2. Effects of the morphology and size of Fe_3O_4 microparticles

A series of contrastive experiments was conducted at 180 °C for 16 h to investigate the formation of Fe_3O_4 with an adjustable morphology.

The concentration of NaOH in the reaction system is an important factor that determines the morphology of the final product. The scanning electron microscopy (SEM) images of the products in the absence of $C_2H_6O_2$ and different NaOH concentrations are shown in Fig. 2.

Fig. 2a shows the irregularly shaped particles obtained when the concentration of NaOH is 0.15 M. Increasing the NaOH concentration to 0.30 M leads to the formation of inhomogeneous octahedral particles (Fig. 2b). A 0.50 M NaOH concentration produces homogeneous Fe_3O_4 microoctahedrons consisting of eight equilateral triangular sheets (Fig. 2c). And the statistical edge size distribution of Fe_3O_4 octahedrons is illustrated in Fig. 3a. It shows that most of the grains have sizes in the range of 3–4 μm. With the further increase of NaOH concentration (0.75 M), the size distribution of the octahedral Fe_3O_4 particles becomes wider (data not shown). Based on these experimental results, Fe_3O_4 microoctahedrons can be formed when the concentration of NaOH ranges from 0.30 to 0.75 M, and the optimal concentration is 0.5 M. However, very high concentrations of NaOH (>0.75 M) produce different morphologies, including octahedrons, sheets, and irregularly shaped particles (Fig. 2d).

It can be seen that the NaOH concentration in the reaction plays a key role in determining the shapes of the products. The pH possibly changes the chemical potential in the reaction system and affects the growth rate of the Fe_3O_4 crystals in different directions [33,34], leading to the difference in morphologies. Zhao and co-workers reported that the chemical potential of octahedra should be generally higher than that of other morphologies if the unit cell of the corresponding crystal structure was not highly distorted along a certain axis [28]. In our experiment, the higher chemical potential can be obtained by increasing the concentration of OH^- ions [23]. At relative low concentration of NaOH (0.30 M), the chemical potential cannot be high enough in the reaction, leading to the formation of inhomogeneous octahedral particles. With the increase of NaOH concentration (0.50 M), the chemical potential is enhanced and the homogeneous Fe_3O_4 microoctahedrons are obtained. Furthermore, the OH^- ions can also change the crystal surface energy. It has been reported that at relative high concentration of OH^- ions, the {1 1 1} lattice planes of Fe_3O_4 had a higher energy than other planes. Similarly, the growth rate of the {1 1 1} lattice planes was slower than that of other planes because the {1 1 1} planes had been selectively covered by the hydrazine hydrate molecules. Consequently, octahedral Fe_3O_4 enclosed by {1 1 1} lattice planes could be produced [23]. In our current study, with the further increase of NaOH concentration (0.75 M), the crystal seeds of Fe_3O_4 are formed rapidly, and the crystal seeds are too many to grow uniformly in aqueous solution, leading to the formation of Fe_3O_4 microoctahedrons with a broad size distribution. The nucleation rate of Fe_3O_4 crystal seeds is further accelerated in the very high concentrations of NaOH (>0.75 M). And the growth rate of Fe_3O_4 crystals in different lattice facets may be affected. As a result, the Fe_3O_4 microparticles with different morphologies are obtained.

$C_2H_6O_2$ also affects the shape of Fe_3O_4 in the current reaction system. Fig. 4 shows the SEM images of the Fe_3O_4 samples obtained at 180 °C for 16 h in the presence of 0.50 M NaOH and different amounts of $C_2H_6O_2$. The morphology of Fe_3O_4 becomes octahedral (Fig. 4a) when 5 mL $C_2H_6O_2$ is added to the solution, and the edge size of the octahedral particles is about 2–2.5 μm, which is less than that of the particles obtained in the absence of $C_2H_6O_2$ (Fig. 2c). This result can be attributed to the adsorption of $C_2H_6O_2$ on the surface of the Fe_3O_4 crystals, which restrains particle growth. The increase in $C_2H_6O_2$ in the reaction system increases the formation of cubic particles (Fig. 4b and c). A 20 mL solution of $C_2H_6O_2$ produces homogeneous cubic particles. The statistical edge size distributions of octahedral and cubic particles are illustrated in Fig. 3b and c. It shows that most of the octahedral and cubic grains have sizes in the range of 2.0–2.5 μm with a uniform shape. Meanwhile, the selected area electron diffraction (SAED) patterns of the edges of the octahedral and cubic Fe_3O_4 obtained using different volumes of $C_2H_6O_2$ solution (5 and 20 mL) are shown in Fig. 5. The octahedral (Fig. 5a) and cubic (Fig. 5b) Fe_3O_4 both exhibit single-crystal features, and the spots for the octahedral or cubic Fe_3O_4 reveal the {1 1 1} or {1 0 0} lattice planes as basal surfaces, respectively.

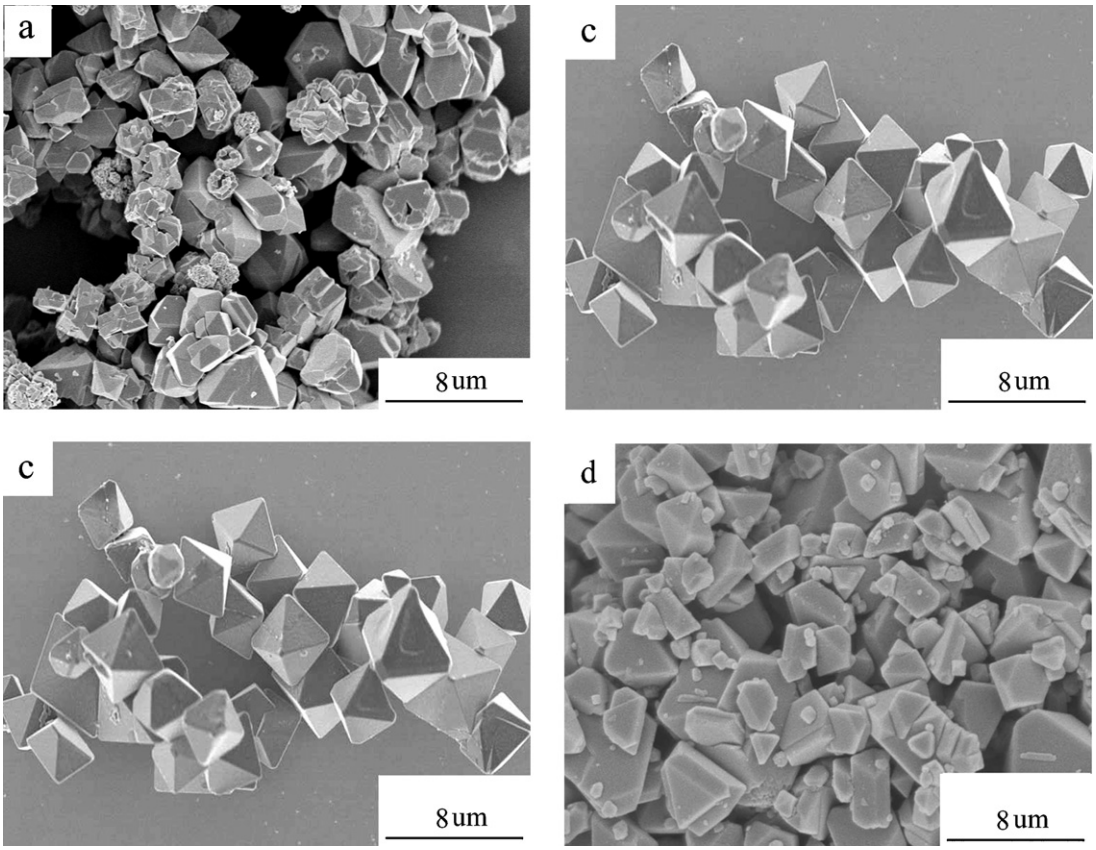

Fig. 2. SEM images of the products prepared in the absence of $C_2H_6O_2$ and different NaOH concentrations (a: 0.15 M; b: 0.30 M; c: 0.50 M; d: 1.00 M).

It is known that a single-crystal particle usually has a specific shape because it has to been closed by lower-energy crystallographic facets [12]. The general sequence of the surface energies of Fe_3O_4 is $\gamma\{1\,1\,0\} > \gamma\{1\,0\,0\} > \gamma\{1\,1\,1\}$ [18]. According to the surface free energy minimization principle, a single-crystal Fe_3O_4 should be enclosed by {1 1 1} planes. Generally, the ratio of the growth rate in the <1 0 0> direction to that in <1 1 1> determines the shape of the fcc crystal, and a faster growth on the <1 0 0> direction can lead to the formation of octahedral crystals [35]. In the current study, $C_2H_6O_2$, which acts as a capping agent, is adsorbed on the high-energy facets of the particles. The overall specific surface energy of crystallographic facets is more or less reduced, leading to the decrease of growth rate in the surface reaction. The ratio of the growth rates in different directions can be affected by the adsorption of $C_2H_6O_2$ onto particular crystallographic facets, which inhibits the growth in a particular crystallographic direction [36]. Because the energy of {1 1 0} facets is higher than those of {1 0 0} and {1 1 1} facets, a 5 mL solution of $C_2H_6O_2$ can preferentially adsorb on the {1 1 0} facets and then reduce the energy and growth rates in these facets. By contrast, the growth rate of the formed primary Fe_3O_4 seeds in {1 0 0} faces are increased and faster than that in {1 1 1}, which leads to the formation of octahedral Fe_3O_4 microparticles. A sufficiently high amount of $C_2H_6O_2$ can be further adsorbed on the {1 0 0} facets and decrease the growth rate in the <1 0 0> direction. As a result, the growth rate in the <1 1 1> direction is higher than that in <1 0 0>, leading to the formation of Fe_3O_4 cubic microparticles [35].

A time-dependent experiment was conducted to investigate the mechanism of formation of the cubic structure. Figs. 6 and 7 show the XRD patterns and SEM images, respectively, of samples obtained at 180 °C for 4, 8, and 12 h. A cubic spinel Fe_3O_4 structure is formed after 4 h, and Fe_3O_4 particles with higher crystallinity are obtained as the reaction proceeds (Fig. 6b and c).

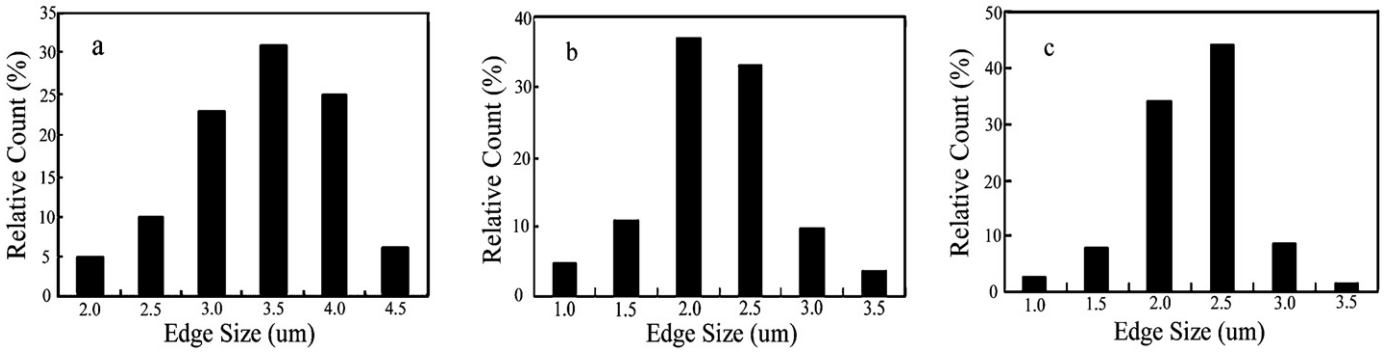

Fig. 3. Edge size distribution histograms of the Fe_3O_4 microparticles (a: NaOH 0.5 M, $C_2H_6O_2$ 0 mL; b: NaOH 0.5 M, $C_2H_6O_2$ 5 mL: c: NaOH 0.5M, $C_2H_6O_2$ 20 mL).

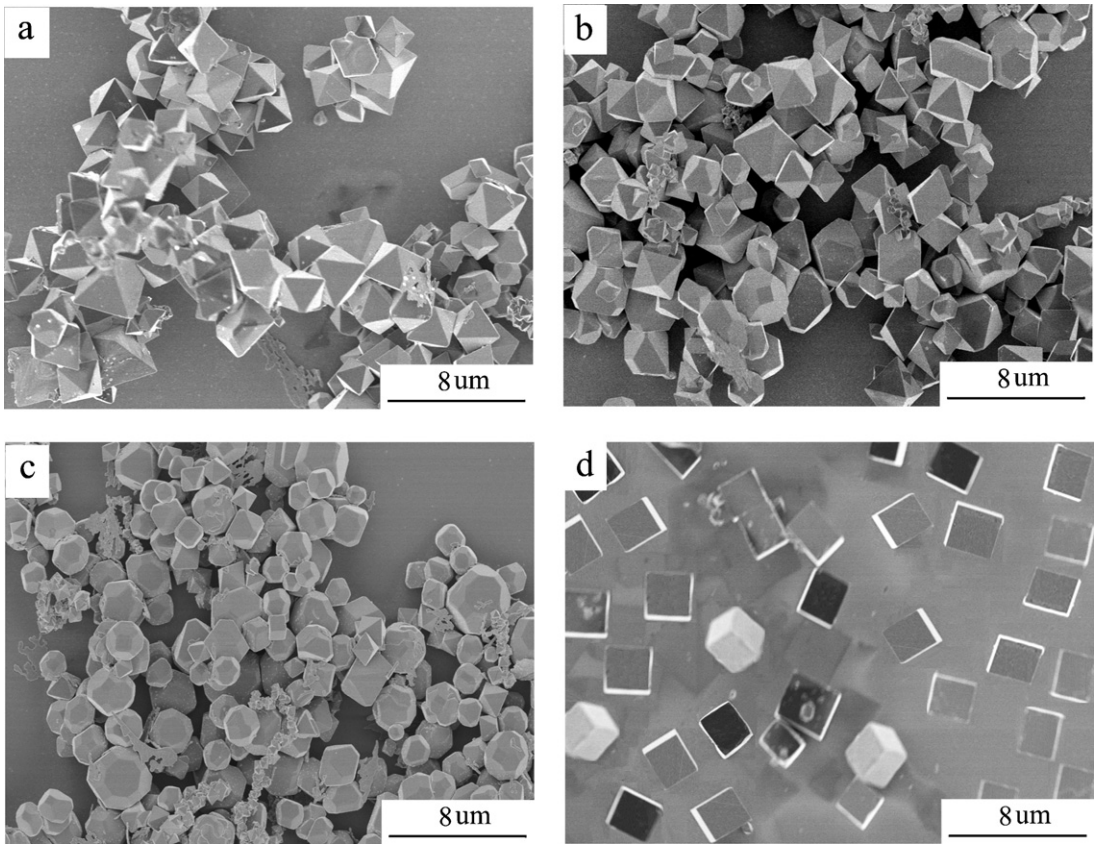

Fig. 4. SEM images of the Fe_3O_4 samples obtained with different amount of $C_2H_6O_2$ solution (a: 5 mL; b: 10 mL; c: 15 mL; d: 20 mL).

Prolonging the reaction time changes the morphologies of the samples. Fe_3O_4 particles with a nearly spherical morphology (Fig. 7a) appear after 4 h of growth reaction at 180 °C. Some cubic particles, with a number of particles attached, are produced after 8 h (Fig. 7b). Cubic particles dominate the products after 12 h (Fig. 7c), and homogeneous cubic particles are obtained after 16 h (Fig. 4d).

This process of crystal growth and morphological evolution can be described by Ostwald ripening, which involves the growth of large particles at the expense of smaller ones. This process is driven by the tendency of the solid phase in the system to adjust to achieve a minimum total surface free energy. Thus, nearly spherical Fe_3O_4 particles are formed first under hydrothermal conditions. When the reaction time is prolonged, the initially spherical particles gradually dissolve in the solution, and cubic particles eventually form and grow. The formation and growth of the cubic Fe_3O_4 may be via a solid–solution–solid process.

3.3. Magnetic properties

The magnetic properties of Fe_3O_4 octahedrons with 3–4 μm (O1) and 2–2.5 μm (O2) edge sizes and Fe_3O_4 cubes with 2–2.5 μm (C) edge sizes were investigated. The O1, O2 and C samples were obtained at 180 °C for 16 h in the presence of 0.50 M NaOH and different amounts of $C_2H_6O_2$ (O1: 0 mL; O2: 5 mL; C: 20 mL).

Fig. 8 shows the M (H) curves for octahedral Fe_3O_4 with different crystalline sizes (O1 and O2) and cubic Fe_3O_4 (C) at room temperature. All samples exhibit ferromagnetic behaviors, although the hysteresis loops in the saturation magnetization (M_s), remanent

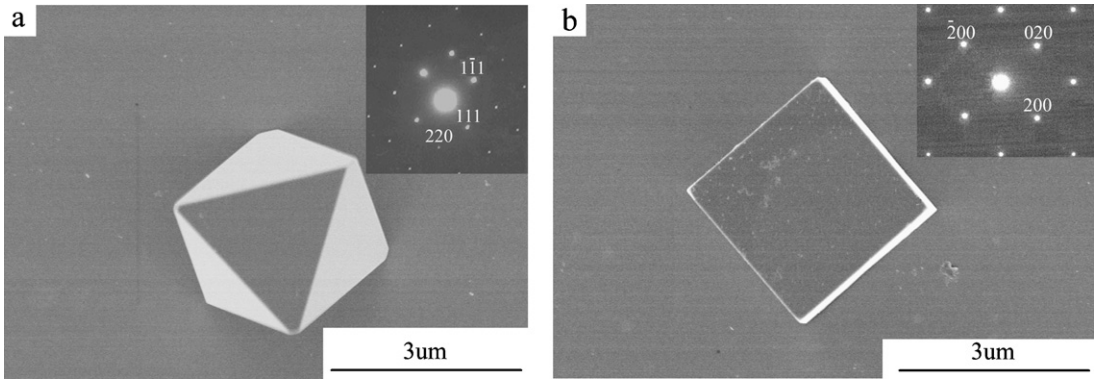

Fig. 5. SEM images and SAED patterns of the edges of the octahedral and cubic Fe_3O_4 (a: octahedral; b: cubic).

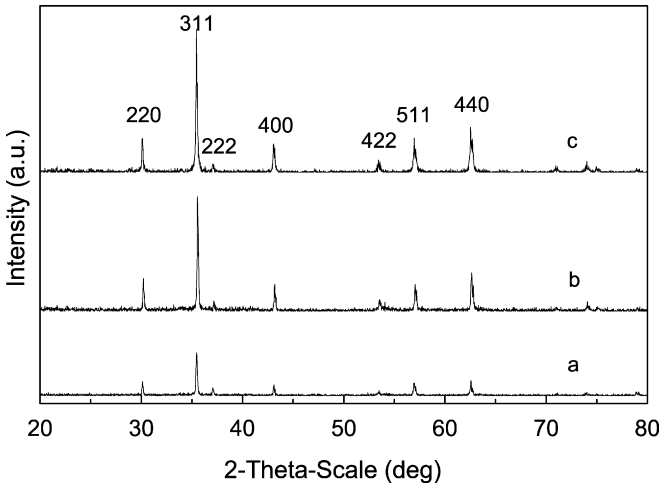

Fig. 6. XRD patterns of samples obtained at different times: (a) 4 h; (b) 8 h; (c) 12 h.

Table 1
Magnetic parameters of octahedral Fe_3O_4 with different crystalline size (O1 and O2) and cubic Fe_3O_4 (C).

Samples	M_s (emu/g)	M_r (emu/g)	H_c (Oe)
O1	101.3	12.2	120.2
O2	81.9	10.4	115.4
C	87.9	8.9	76.8

magnetization (M_r), and coercivity (H_c) are different. The corresponding magnetic parameters are listed in Table 1.

It can be seen that the M_s of the octahedral Fe_3O_4 (O1) is highest among all samples and is a little higher than that of the bulk Fe_3O_4 (85–100 emu/g [37]). And the M_s of O2 is lower than that of the bulk Fe_3O_4. Some studies revealed that the properties of magnetic materials were greatly influenced by factors such as size, structure, morphology, crystallinity, surface effects, etc. [17,26,29,38]. Among them, surface effects, such as spin canting, partial oxidation, and deviations from stoichiometry or adsorbed molecules are usually held responsible for values of M_s smaller than that for the

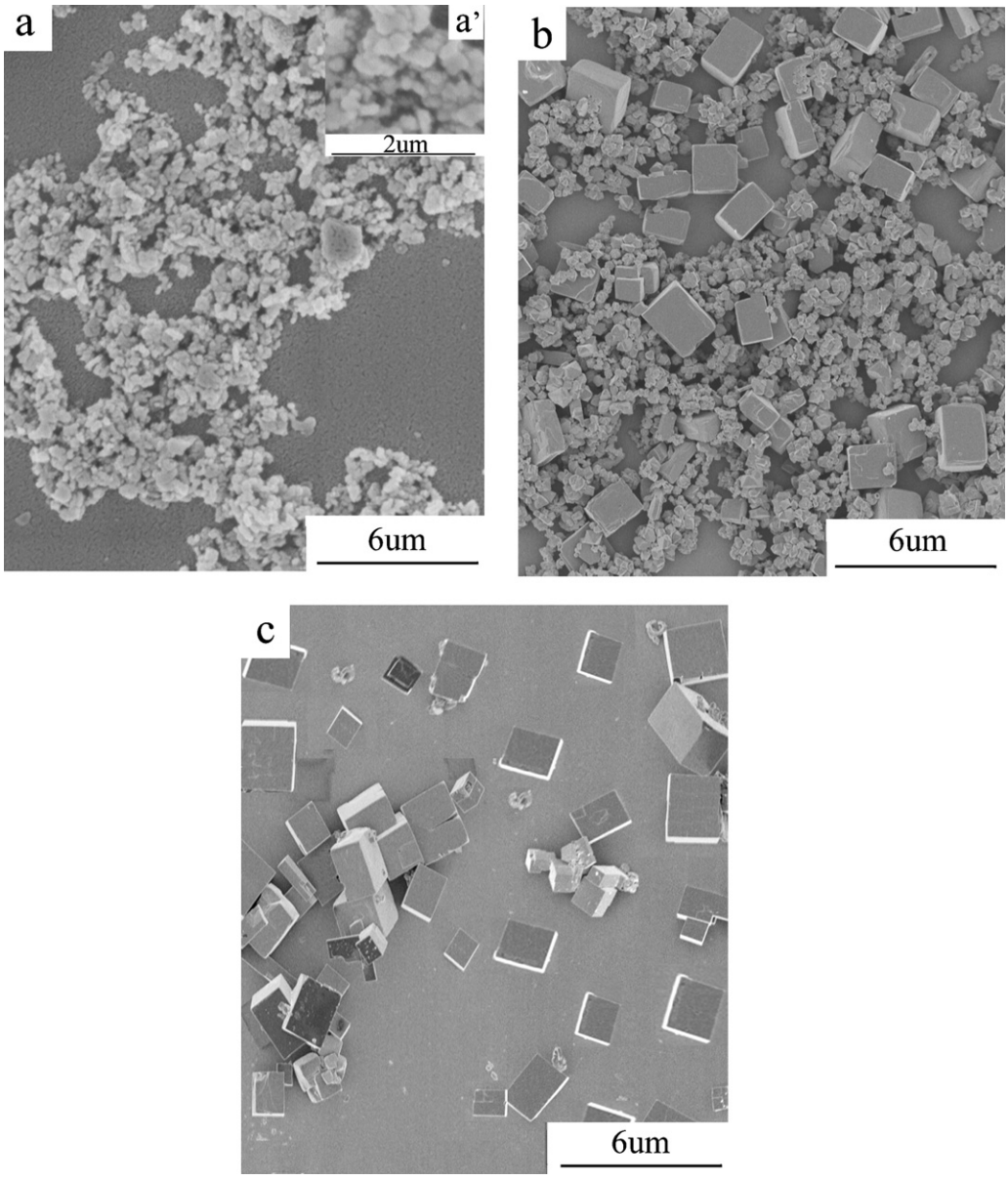

Fig. 7. SEM images of samples obtained at different times: (a) 4 h; (a′) enlarged magnetization, 4 h; (b) 8 h; (c) 12 h.

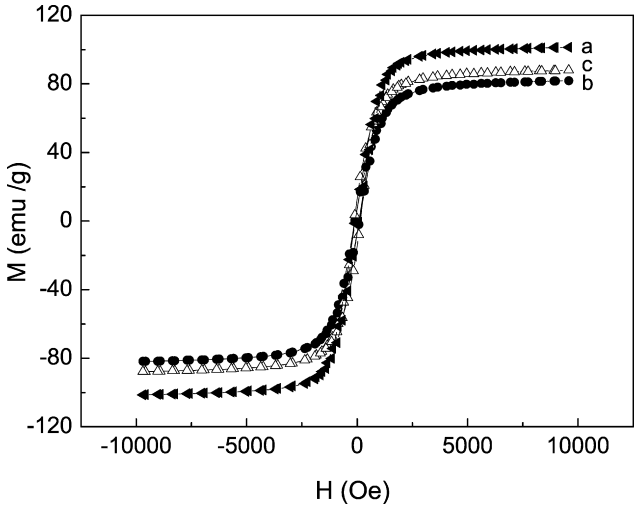

Fig. 8. Magnetization curves of octahedral Fe_3O_4 with different crystalline size (a: O1, b: O2) and cubic Fe_3O_4 (c: C).

bulk material. Vereda et al. reported that surface effects became more important as the average size of the particles decreased, and therefore explained why the lower values of M_s were observed the smaller the particle size became [32]. In the present work, surface effects may play an important role in the difference for the saturation magnetization between O1 and O2. The O2 sample is obtained in the presence of ethanediol. The ethanediol can adsorb on the exposed faces of the Fe_3O_4 and form a magnetically dead layer, leading to the decrease in M_s. On the other hand, Fe_3O_4 crystallizes in cubic structure with iron in two different valence states, the Fe_3O_4 can be written in the form of $FeO{\cdot}Fe_2O_3$ with Fe(II) as FeO and Fe(III) as Fe_2O_3. The Fe(III) occupies the tetrahedral sites and half the octahedral sites, with Fe(II) occupying the other half. The magnetic moments on the octahedral sites are anti-ferromagnetic, while on the tetrahedral sites they are ferromagnetically aligned. The differences in crystallization process could influence the distribution of Fe(II) octahedral and Fe(III) octahedral and then the super exchange interaction between ferric ions [39]. In addition, the magnetic properties of samples can also be related to the morphology of the particles [16,23,40]. As can be seen from Table 1, cubic Fe_3O_4 particles have the smallest H_c values because of their higher symmetry and smaller shape anisotropy compared with other samples. Therefore, the H_c of the regular cubic Fe_3O_4 particles is smaller compared with those of other samples. Further work will be done in our laboratory.

4. Conclusions

Fe_3O_4 microparticles with various morphologies and sizes were successfully prepared using a simple hydrothermal process. The morphology and size of Fe_3O_4 depended on the NaOH and $C_2H_6O_2$ concentrations. Octahedral Fe_3O_4 microparticles were formed when the concentration of NaOH ranged from 0.30 to 0.75 M. When a small amount of $C_2H_6O_2$ was added to the reaction system, the size of the Fe_3O_4 octahedrons decreased. The morphology of Fe_3O_4 changed from octahedral to cubic when the $C_2H_6O_2$ concentration was increased. The formation and growth of cubic Fe_3O_4 particles may have been via a solid–solution–solid process. The octahedral and cubic Fe_3O_4 showed single-crystal structures. In addition, the as-prepared Fe_3O_4 microparticles with various morphologies and sizes exhibited ferromagnetic behaviors.

Acknowledgments

This work was financially supported by the National Natural Science Foundation of China (21077031), the Natural Science Foundation of Hebei Province (08B011) and the Key Laboratory of Photochemical Conversion and Optoelectronic Materials, TIPC, CAS (PCOM201110).

References

[1] L. Chen, C. Zhao, Y. Zhou, H. Peng, Y. Zheng, J. Alloys Compd. 504 (2010) L46–L50.
[2] J. Chen, F. Wang, K. Huang, Y. Liu, S. Liu, J. Alloys Compd. 475 (2009) 898–902.
[3] S. Wu, A. Sun, F. Zhai, J. Wang, W. Xu, Q. Zhang, A. Volinsky, Mater. Lett. 65 (2011) 1882–1884.
[4] B. Veriansyah, J.-D. Kim, B.K. Min, J. Kim, Mater. Lett. 64 (2010) 2197–2200.
[5] G. Tonga, W. Wua, J. Guan, H. Qian, J. Yuan, W. Li, J. Alloys Compd. 509 (2011) 4320–4326.
[6] J. Feng, J. Mao, X. Wen, M. Tu, J. Alloys Compd. 509 (2011) 9093–9097.
[7] Y.Y. Zheng, X.B. Wang, L. Shang, C.R. Li, C. Cui, W.J. Dong, W.H. Tang, B.Y. Chen, Mater. Charact. 61 (2010) 489–492.
[8] T. Gong, D. Yang, J. Hu, W. Yang, C. Wang, J.Q. Lu, Colloids Surf. A: Physicochem. Eng. Aspects 339 (2009) 232–239.
[9] X. Yu, J. Wan, Y. Shan, K. Chen, X. Han, Chem. Mater. 21 (2009) 4892–4898.
[10] X. Yu, Y. Shan, G. Li, K. Chen, J. Mater. Chem. 21 (2011) 8104–8109.
[11] S. Ni, X. Sun, X. Wang, G. Zhou, F. Yang, J. Wang, D. He, Mater. Chem. Phys. 124 (2010) 353–358.
[12] L. Zhao, H. Zhang, J. Tang, S. Song, F. Cao, Mater. Lett. 63 (2009) 307–309.
[13] D.E. Zhang, X.J. Zhang, X.M. Ni, J.M. Song, H.G. Zheng, Cryst. Growth Des. 7 (2007) 2117–2119.
[14] D. Peng, S. Beysen, Q. Li, J. Jian, Y. Sun, J. Jiwuer, Particuology 7 (2009) 35–38.
[15] L. Zhang, Q. Li, S. Liu, M. Ang, M.O. Tade, H.-C. Gu, Adv. Powder Technol. 22 (2011) 532–536.
[16] V.G. Pol, L.L. Daemen, S. Vogel, G. Chertkov, Ind. Eng. Chem. Res. 49 (2010) 920–924.
[17] X.F. Qu, G.T. Zhou, Q.Z. Yao, S.Q. Fu, J. Phys. Chem. C 114 (2010) 284–289.
[18] L. Zhang, R. He, H.-C. Gu, Mater. Res. Bull. 41 (2006) 260–267.
[19] C. Guo, Y. Hu, H. Qian, J. Ning, S. Xu, Mater. Charact. 62 (2011) 148–151.
[20] B.J. Wang, Q. Chen, C. Zeng, B. Hou, Adv. Mater. 16 (2004) 137–140.
[21] A. Yan, Y. Liu, Y. Liu, X. Li, Z. Lei, P. Liu, Mater. Lett. 68 (2012) 402–405.
[22] G. Zou, K. Xiong, C. Jiang, H. Li, T. Li, J. Du, Y. Qian, J. Phys. Chem. B 109 (2005) 18356–18360.
[23] X. Yu, Y. Shan, B. Du, K. Chen, CrystEngComm 13 (2011) 1525–1530.
[24] D.B. Yu, X.Q. Sun, J.W. Zou, Z.R. Wang, F. Wang, K. Tang, J. Phys. Chem. B 110 (2006) 21667–21671.
[25] K.C. Chin, G.L. Chong, C.K. Poh, L.H. Van, C.H. Sow, J.Y. Lin, A.T.S. Wee, J. Phys. Chem. C 111 (2007) 9136–9141.
[26] X. Li, Z. Si, Y. Lei, J. Tang, S. Wang, S. Su, S. Song, L. Zhao, H. Zhang, CrystEngComm 12 (2010) 2060–2063.
[27] R. Liu, Y. Zhao, R. Huang, Y. Zhao, H. Zhou., Eur. J. Inorg. Chem. 28 (2010) 4499–4505.
[28] L. Zhao, H. Zhang, Y. Xing, S. Song, S. Yu, W. Shi, X. Guo, J. Yang, Y. Lei, F. Cao, Chem. Mater. 20 (2008) 198–204.
[29] X. Wang, Z. Zhao, J. Qu, Z. Wang, J. Qiu, Cryst. Growth Des. 10 (2010) 2863–2869.
[30] R. Chen, G. Song, Y. Wei, J. Phys. Chem. C 114 (2010) 13409–13413.
[31] T. Belin, N. Guigue-Millot, T. Caillot, D. Aymes, J.C. Niepce, J. Solid State Chem. 163 (2002) 459–465.
[32] F. Vereda, J. d. Vicente, d.P.M. María, F. Rull, R. Hidalgo-Alvarez, J. Phys. Chem. C 112 (2008) 5843–5849.
[33] J. Yu, A. Kudo, Adv. Funct. Mater. 16 (2006) 2163–2169.
[34] X. Yu, K. Chen, Mater. Sci. Eng. B 176 (2011) 750–755.
[35] Z.L. Wang, Adv. Mater. 10 (1998) 13–30.
[36] V.F. Puntes, D. anchet, C.K. Erdonmez, A.P. Alivisatos, J. Am. Chem. Soc. 124 (2002) 12874–12880.
[37] S. Xuan, L. Hao, W. Jiang, L. Song, Y. Hu, Z. Chen, L. Fei, T. Li, Cryst. Growth Des. 7 (2007) 430–434.
[38] G.C. Xi, Y.K. Liu, X.Q. Wang, X.Y. Liu, Y.Y. Peng, Y.T. Qian, Cryst. Growth Des. 6 (2006) 2567–2570.
[39] J. Wang, J. Sun, Q. Sun, Q. Chen, Mater. Res. Bull. 38 (2003) 1113–1118.
[40] L. Gu, H. Shen, J. Alloys Compd. 472 (2009) 50–54.